An Asymmetric Sampled Grating Laser and Its Application to Multi-Wavelength Laser Array

Sang-Wan Ryu and Jeha Kim

We propose an asymmetric sampled grating laser and a multi-wavelength laser array associated with it. Asymmetric sampling periods combined with an index shifter make it possible to use first order reflection for lasing operations. With the structure of our design, we achieved a simple fabrication procedure as well as a high yield without using complex and time-consuming e-beam lithography for multi-period gratings. We analyzed the effect of mirror coating by numerical analysis to improve single mode and power extraction performance. By using high reflection-antireflection coatings, we obtained high power extraction efficiency without degradation of the single mode property. For the multi-wavelength laser array, to gain wavelength control, we varied the sampling periods from one laser to an adjacent laser across the array. With this approach, we showed the feasibility of an array of up to 30 channels with 100 GHz wavelength spacing.

Manuscript received Sept. 29, 2001; revised Aug. 7, 2002.

Sang-Wan Ryu (phone: +82 42 860 1158, e-mail: sangwan@etri.re.kr) and Jeha Kim (e-mail: jeha@etri.re.kr) are with Integrated Optical Source Team, ETRI, Daejeon, Korea.

I. INTRODUCTION

Recent progress in wavelength division multiplexing (WDM) technologies for broadband fiber optic communication systems has revealed a need for a multiple wavelength light source [1]-[3]. The multi-wavelength transmitters for WDM systems are currently built with multiple discrete lasers [2]. However, integrating discrete lasers for a multi-wavelength laser suffers from a high packaging cost and the burden of multiple alignments between laser diodes and optical fibers. The monolithic integration of lasers into a multi-wavelength laser array (MLA) has been presented as a promising approach to reducing the cost per wavelength so that the cost of packaging and of the required pigtail optics can be shared by a large number of wavelengths [3].

The conventional approaches to fabricating an MLA require a way to vary the Bragg wavelengths of constituent distributed feedback (DFB) lasers across the array; this can be realized by several techniques, such as multiple holographic exposure, e-beam writing [4], and selective area growth [5]. However, most of the existing approaches are not applicable to mass production because of complex fabrication procedures and difficulties in accurate control of the wavelength spacing. It is highly desirable to vary the lasing wavelength of the MLA without using complicated and expensive procedures.

Here, we present a novel approach to realize the MLA by using a sampled grating. The sampled grating is a versatile tool for tailoring the optical characteristics of a grating structure [6], [7]. It is basically a uniform periodic corrugation separated with uncorrugated sampled regions, so its fabrication is easier than that of a pitch-modulated [8] or coupling coefficient-modulated [9] grating. The key concept of the proposed approach is to utilize a first order reflection of the sampled grating for the

lasing operation. Although it is hard to vary the Bragg wavelength itself across the array, the wavelength of the first order reflection can be controlled by simply adjusting the period of the sampled grating.

This paper presents the design and theoretical analysis of an MLA associated with an asymmetric sampled grating (ASG) laser. We obtained the design guidelines and criteria for stable single mode operation by controlling the mirror reflectivity and the coupling coefficient. In addition, various laser performances were investigated in terms of such parameters as threshold gain and power extraction efficiency.

II. MATHEMATICAL FORMULATION

A convenient way to calculate longitudinal modes of a DFB laser and a distributed Bragg reflector (DBR) laser is to use a transfer matrix method [10]. This method supposes that there are forward and backward traveling fields on the right-hand and left-hand sides of a scattering element. The scatterer transforms the fields into each other, and the transition can be defined by using a transfer matrix **T** expressed as follows.

$$\begin{bmatrix} a_1 \\ b_1 \end{bmatrix} = \mathbf{T} \begin{bmatrix} a_2 \\ b_2 \end{bmatrix}, \quad with \quad \mathbf{T} = \begin{bmatrix} T_{11} & T_{12} \\ T_{21} & T_{22} \end{bmatrix}. \tag{1}$$

Here, a and b represent the forward and backward traveling fields, respectively. The subscripts 1 and 2 indicate either the right-hand or left-hand sides of the scatterer where the field exists.

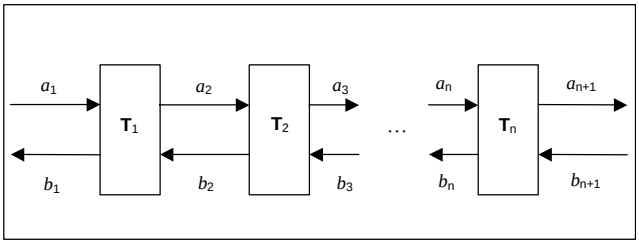

Fig. 1. Schematic diagram of scattering centers ($\mathbf{T}_n$) which scatter right (a_n) and left (b_n) propagating fields into each other.

If several scattering elements are given as in Fig. 1, (1) can be expanded to describe the interaction between the fields as in (2). The combined effect of the scattering elements is then formulated by a total transfer matrix ($\mathbf{T}^{tot}$). $\mathbf{T}^{tot}$ in (3) can be obtained simply by the product of all the individual matrices that describe a physical operation of its own.

$$\begin{bmatrix} a_1 \\ b_1 \end{bmatrix} = \mathbf{T_1} \begin{bmatrix} a_2 \\ b_2 \end{bmatrix} = \mathbf{T_1 T_2} \begin{bmatrix} a_3 \\ b_3 \end{bmatrix} = \cdots = \mathbf{T_1 T_2 T_3} \cdots \mathbf{T_n} \begin{bmatrix} a_{n+1} \\ b_{n+1} \end{bmatrix} \tag{2}$$

$$\mathbf{T}^{tot} = \mathbf{T_1 T_2 T_3} \cdots \mathbf{T_n} \tag{3}$$

The transfer matrix method can be used to calculate the threshold gain and wavelength of the DFB and DBR lasers by observing the total transfer function $\mathbf{T}^{tot}$ of the laser cavity [11]. The laser cavity is divided into small segments for which the transfer matrix is quite simple. $\mathbf{T}^{tot}$ is then calculated by multiplying the elemental matrices along the cavity. Defining the transfer matrix allows us to determine various parameters of the lasing condition. The zeros of T^{tot}_{11} indicate the existence of an output field while any input field is absent, which is possible when lasing action occurs. In the numerical calculation, we try to obtain numbers that make T^{tot}_{11} zero as we change the operating condition by varying the optical gain and operating wavelength. Those numbers that set T^{tot}_{11}=0 become the desired threshold values. This method is particularly useful in determining the threshold gain margin of modes. Even after one mode reaches the threshold, the gain can still be increased to look for the next mode to reach the threshold at another wavelength.

The difference of the threshold gain (Δg) between the main mode and the main submode is an important parameter in determining the single mode behavior of a laser. Please note that the Δg is the power gain not the field gain. Usually the product of Δg and the cavity length (L) is a measure of single longitudinal mode stability. A large ΔgL is needed to suppress the mode competition sufficiently. The single mode device is realized when $\Delta gL > 0.3$, that is, it is large enough to get a stable side mode suppression ratio (SMSR) of 30 dB over a wide temperature and power range [11], [12].

When the single mode criterion $\Delta gL > 0.3$ is fulfilled in the calculation, we can derive power extraction efficiency from the total transfer matrix. It is defined as the ratio of the major output power to the sum of two outputs from both facets. The efficiency would take a value of between 0.5 and 1. A value of 0.5 means that the power is equally allocated to both facets while a value of 1 implies the ideal case in which all the power is emanating from one of the facets. The power extraction efficiency can be obtained directly from a coefficient of $\mathbf{T}^{tot}$ using the relation of $a_1/b_{n+1} = |T^{tot}_{21}|^2$ evaluated in the condition of the threshold.

In the following simulation, we investigated the effect of the mirror reflectivity, coupling coefficient, and device length, to obtain the optimum laser properties. The results were used to design the high performance MLA with the ASG laser.

III. SIMULATION RESULTS OF THE ASG LASER

The structure of an ASG laser is schematically shown in Fig. 2(a). The figure shows the cross-sectional view along the laser

cavity. The laser consists of two sampled grating mirrors at sections A and B of different sampling periods. Basically a sampled grating is the periodic structure of a grating separated by a blank space. Thus a segment of a grating is the building block of the sampled grating. It is therefore important to properly choose the grating period for the device. We set the period at 240 nm for all the grating regions so that we could fabricate it with a single holographic exposure. The Bragg wavelength (λ_o) is related to the grating period (Λ) and the effective index (n_{eff}) as follows.

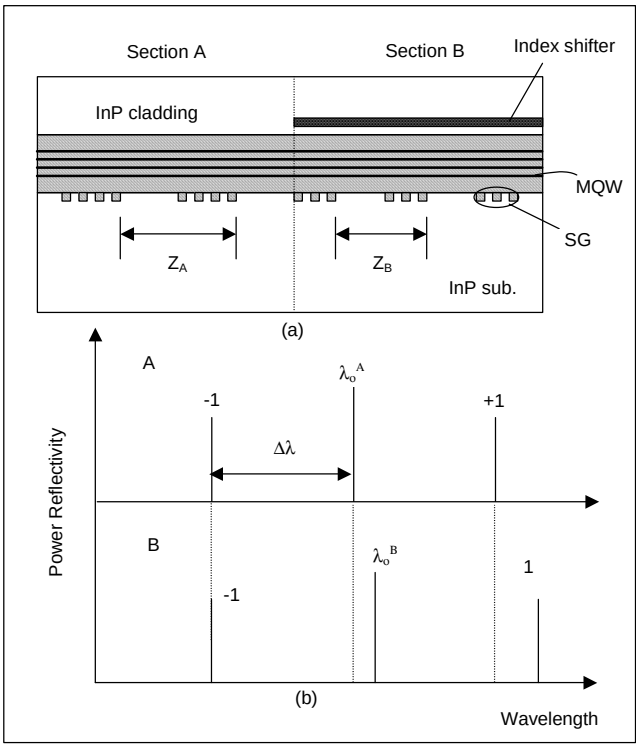

Fig. 2. (a) Schematic structure of the ASG laser. (b) Reflection spectra of the sampled grating mirrors at sections A and B.

$$\lambda_o = 2\, n_{eff}\, \Lambda \tag{4}$$

The key feature of the proposed structure is the inclusion of an index shifter layer on one part of the two sections with which lasing at the Bragg wavelength is suppressed significantly. The index shifter is an InGaAsP layer with a high refractive index inserted in the InP cladding at section B. As a result, the effective index at section B is increased, and the Bragg wavelength of section B (λ_o^B) can be made different from that of section A (λ_o^A).

Figure 2(b) shows a schematic of the reflection spectra for the sampled grating mirrors. By adjusting the effective index of section B, we could make both reflection peaks of the two mirrors with different sampling periods coincide at the –1st order reflection wavelength. Since the cavity has a minimum threshold gain at that wavelength, lasing would take place at the –1st order reflection wavelength rather than at the Bragg wavelength.

For simulation, a conventional laser active structure including multi-quantum wells was assumed. The effective index method was adopted to find the effective refractive index of the waveguide and the value was used to find Bragg wavelengths as in (4). λ_o^A was set at 1570 nm, while λ_o^B was increased by 5 nm using the index shifter. The index shifter was an InGaAsP (λ_g = 1.1 μm) of 150 nm thickness above the laser active layer. During the incorporation of the index shifter, the waveguide should maintain single mode property in a transverse direction. We found that even an 0.3 μm thick index shifter, twice as thick as the current layer, did not introduce an additional mode to the waveguide.

To control the wavelength of the –1st order peaks, the sampling period at each section was adjusted by considering the relation between the reflection peak spacing ($\Delta\lambda$) and the sampled grating period (Z) as follows.

$$\Delta\lambda = \lambda_o^2 / (2\, n_{eff}\, Z) \tag{5}$$

From (5), Z_A was calculated to be 19.2 μm and Z_B to be 15.4 μm to set the lasing wavelength at 1550 nm. Based on the parameters, the power reflectivity of each section was calculated and the result is shown in Fig. 3. The coupling coefficient of grating (κ) was assumed to be 130 cm^{-1} and the sampling duty (the ratio of the grating area to the non-grating area) was 40%. As we expected, the overlap of high reflection bands took place exactly at the –1st order rather than at the

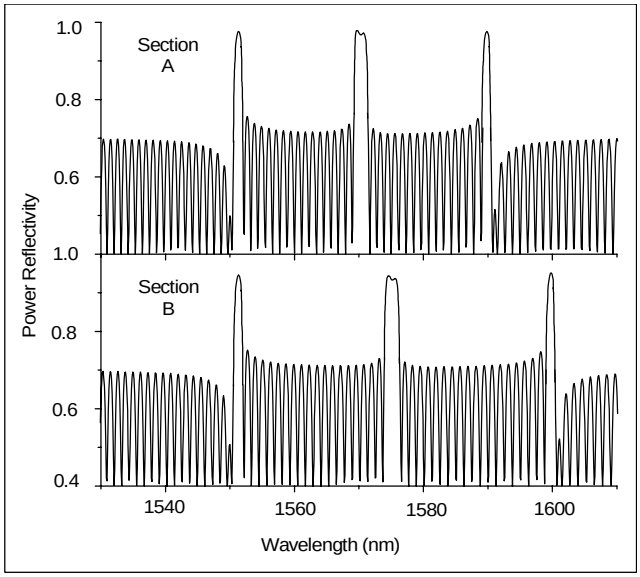

Fig. 3. Comparison of the reflection spectra of sections A and B calculated by the transfer matrix method.

Bragg position. It is clear from Fig. 3 that the amount of separation between the Bragg wavelengths should be adjusted carefully to avoid an overlap between the stop-bands of the Bragg reflections.

We investigated the combined effect of the sampled gratings at both sections by surveying the longitudinal modes for the lasing operation. The gain and the wavelength at threshold are of primary concern for laser performance. It was assumed that the lengths of sections A and B were 300 μm. For simplicity, the phases at both facets (ϕ_1, ϕ_2) were set to 0.

Figure 4 shows the threshold gain versus the wavelength for the asymmetric sampled grating laser for various mirror reflectivities. The baseline of the threshold gain curve came from the Fabry-Perot (FP) modes. The threshold gain of the FP mode was calculated from the reflectivity and it was very close to the baseline value in Fig. 4. Besides the FP modes, several groups of modes originated from different reflection bands of the sampled grating. The modes at around 1550 nm came from the overlapped –1st order reflection, while the modes between 1570–1575 nm originated from the Bragg reflection of either section A or B. Due to the overlap of the –1st order reflection peaks of both sections, the modes around 1550 nm appeared to have the smallest threshold gain, as expected. It should be pointed out, however, that the lasing mode in a given device depends on the spectral profile of the gain material as well. The modes of the –1st order reflection would lase only if the gain peak occurred in the vicinity of that wavelength. When the gain peak is much closer to the Bragg wavelength, the Bragg modes might reach the threshold first. However, if the gain peak is controlled properly, the threshold gain difference between the modes of the –1st order reflection and those of the Bragg reflection can be made much larger.

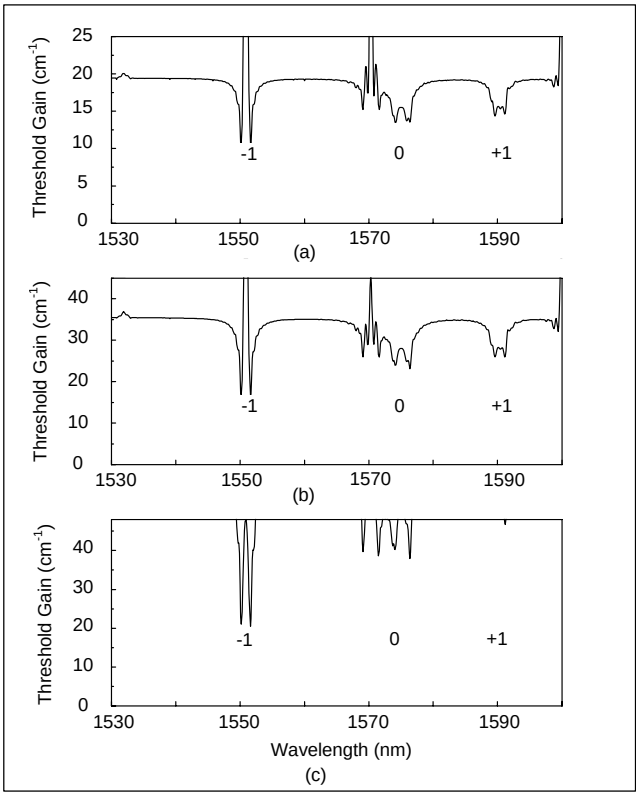

Fig. 4. Calculated threshold gain of ASG laser modes. The effect of AR coatings on mirror facets is included: (a) CL-CL (b) 10%-10% (c) 1%-1%.

In order to prevent the FP cavity modes from interfering with the single mode property, antireflection (AR) coatings were applied on both facets. The effect of AR coatings with various reflectivities was simulated and included in Figs. 4(b) and (c). The calculated Fabry-Perot threshold gain increased to 38 cm^{-1} with an AR coating of 10% reflectivity (Fig. 4(b)) and to 77 cm^{-1} with that of 1% reflectivity (Fig. 4(c)). With the increase of the FP threshold gain, the threshold gain difference between the –1st order modes and the Bragg modes enlarged markedly. As a result, with 1% AR coating, it was enhanced by 17 cm^{-1}.

As shown in Fig. 4, there are two longitudinal modes that locate symmetrically with respect to the center of the stop-band. Mode competition between them is of great concern because it is directly related to the SMSR. For a DFB laser, it is very difficult to define cleaved mirror facets with respect to grating phases, so, a spread in device quality is expected from the uncontrollable facet phase [11], [12]. For the ASG laser, the presence of a no grating region along the laser cavity makes the analysis more complicated. However, we found that even though a mirror facet was formed in the area of no grating, the phase of the reflected wave was still as sensitive to the mirror position as it was in the grating region.

As stochastic analysis has provided reliable performance analysis for the DFB laser, we chose to use it to further investigate the properties of the proposed ASG laser. We calculated the total transfer matrices for 20 × 20 possible combinations of facet phases and found values of the threshold gain difference and the power extraction efficiency for each device. For all possible combinations, the probability of laser performance was obtained statistically.

Figure 5 shows how the stochastic method can be used for the theoretical analysis of an ASG laser. The horizontal axes represent laser parameters, like the threshold gain difference or power extraction efficiency, that are of interest. The vertical axes represent the probability of showing better performance corresponding to the values on the horizontal axes. For the power extraction efficiency, only single mode devices that satisfy the criterion of $\Delta gL > 0.3$ were taken into account, so the values on the probability axis of the power extraction efficiency graphs represent the gross probability of obtaining single mode performance.

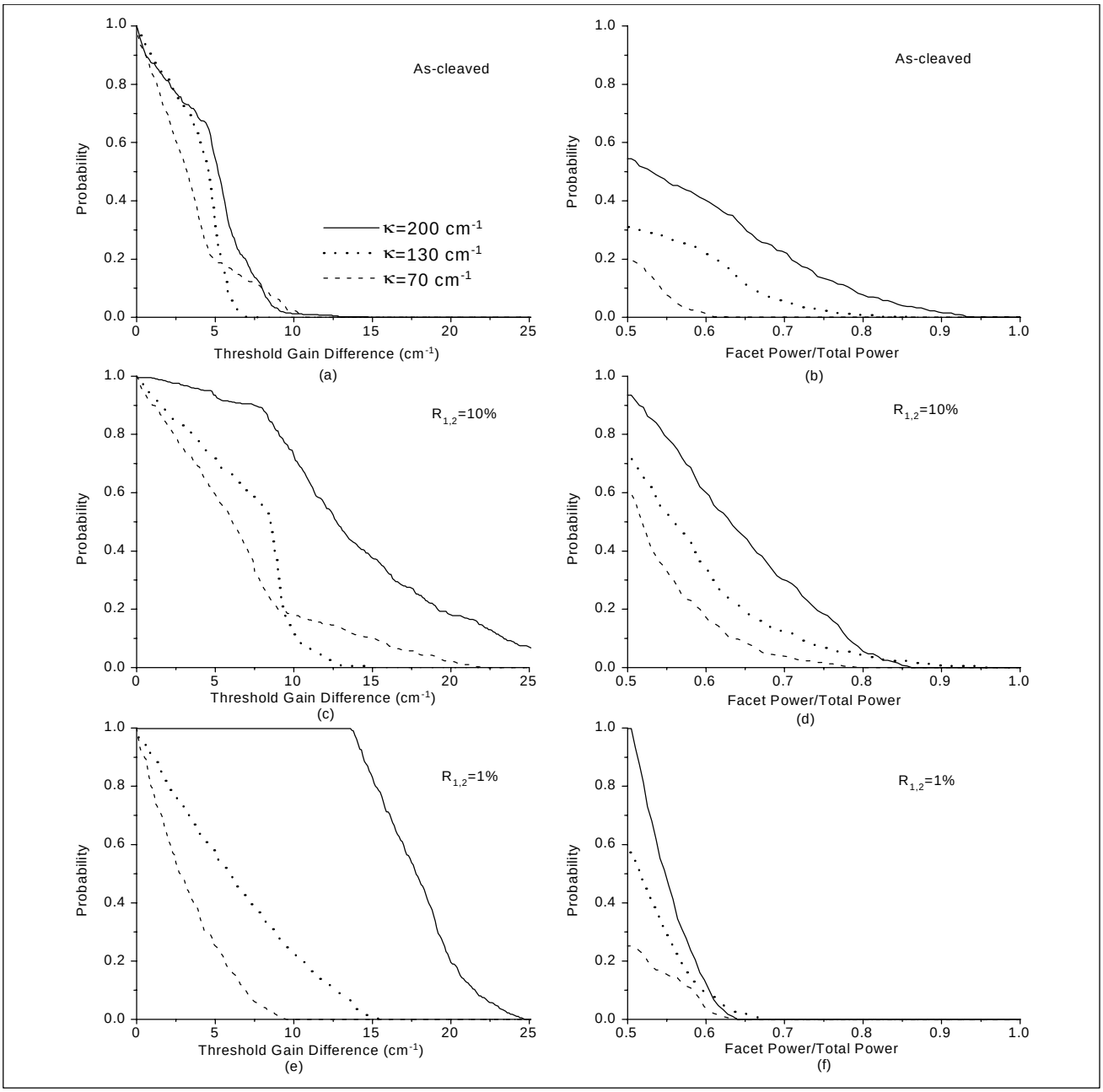

Fig. 5. Theoretical distribution of the threshold gain difference and power extraction efficiency. Accumulated probability of obtaining a device corresponding to laser parameters is displayed. The effect of AR coatings on mirror facets is included. (a), (b): CL-CL; (c), (d): 10%-10%; (e), (f): 1%-1%.

First, we studied the ASG laser with cleaved (CL)-CL facets and the results are shown in Figs. 5(a) and (b). The effect of the coupling coefficient of the grating (κ) was also included. The gross single mode probability was quite low and it took values between 20% and 55% within the range of the coupling coefficients studied (Fig. 5(b)). This result implies that the CL-CL facet structure is not suited for single mode operation with a high yield. It is, however, worth pointing out that the gross single mode probability and the power extraction efficiency increase with the coupling coefficient.

Mirror coating is usually used to improve the single mode probability for a DFB laser. We considered symmetric AR coatings on both facets to study the effect of mirror reflectivity on the performance of the ASG laser. The results are displayed in Fig. 5. Figures 5(c) and (d) are for 10%-10% facet reflectivity and (e) and (f) for 1%-1%. We found that low mirror reflectivity and high κ increased the gross single mode probability, and the probability reached 100% with 1%-1% mirrors and κ=200 cm^{-1}.

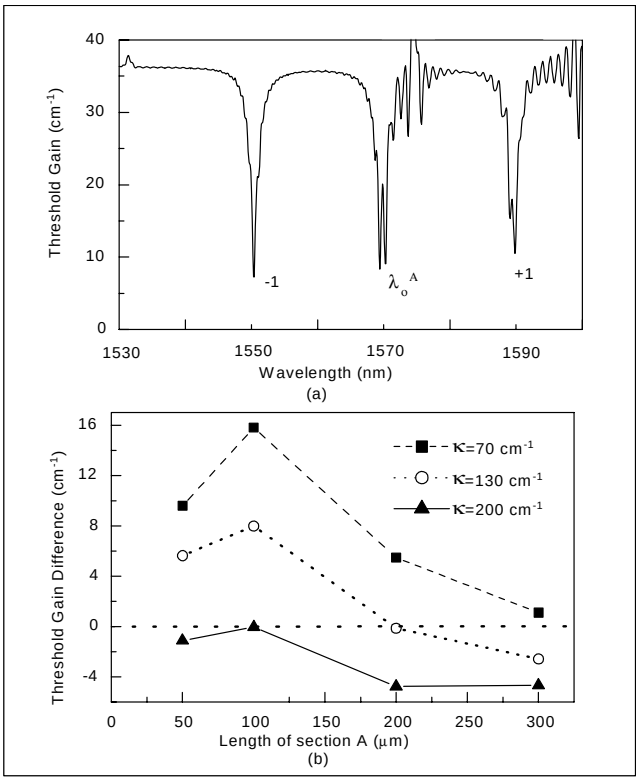

Fig. 6. (a) Calculated threshold gain of the HR-AR coated ASG laser. The length of sections A and B are 300 μm. (b) Threshold gain difference between the –1st modes and the Bragg modes for coupling coefficients.

Our observation implies that the control of the coupling coefficient associated with facet reflectivity is crucial in obtaining a high yield single mode for ASG lasers.

On the other hand, asymmetry in output power, which is mainly due to asymmetric facet phases, was made even smaller by the reduction of reflectivity. The power extraction efficiency was around 0.5 for most of the devices with 1%-1% mirrors (Fig. 5(f)). Larger power extraction efficiency was obtained with CL-CL mirrors, although the gross single mode probability was low (Fig. 5(b)). It was not probable to obtain simultaneously both single mode oscillation and high power extraction efficiency in a structure with symmetric mirror facet reflectivity.

We investigated asymmetric AR-high reflection (HR) coatings as a way of increasing power extraction efficiency while maintaining high single mode yield. Unlike a conventional DFB laser, however, mode competition between the –1st order modes and the Bragg modes should be taken into account in the design of an ASG laser. The lower threshold gain of –1st order modes is only possible when sections A and B contribute equally to the overall reflection spectrum. If asymmetric mirror coatings are given, E-field distribution in the laser cavity loses its symmetry. Therefore, it is necessary to differentiate the contribution of section A from that of section B even though the lengths of sections A and B are identical.

Figure 6(a) shows the modified threshold gain for asymmetric mirror coatings. AR(1%)-HR(90%) coatings at the facets were considered and both sections A and B were set to be 300 μm long. A coupling coefficient of 70 cm^{-1} and $\phi_1=\phi_2=0$ were assumed. The modes around 1570 nm (λ_o at section A) appeared to have a threshold gain comparable to that of the –1st order modes, which was attributed to the contribution of section A's enhanced by asymmetric AR-HR facet coatings.

To make the ASG laser operate at the –1st order modes, we set the length of section A (L_A) to be shorter than L_B. Figure 6(b) shows the difference of threshold gain for several coupling coefficients as a function of L_A. As L_A decreased, the threshold gain difference increased. It has the largest value at L_A of 100 μm. For L_A < 100 μm, the threshold gain difference decreased again because the contribution of section A became too small. The figure also shows that a small coupling coefficient is effective to obtain a large threshold gain difference. When the coupling coefficient is 200 cm^{-1}, the Bragg modes always have a lower threshold gain than the –1st order modes for all L_A's.

We also observed that two symmetric modes around the –1st order reflection band tended to merge into one dominant mode, known as a gap mode, with asymmetric facet coating. In a conventional DFB laser, AR-HR coating is known to improve the SMSR by manipulating the gap mode [13]. Likewise, the

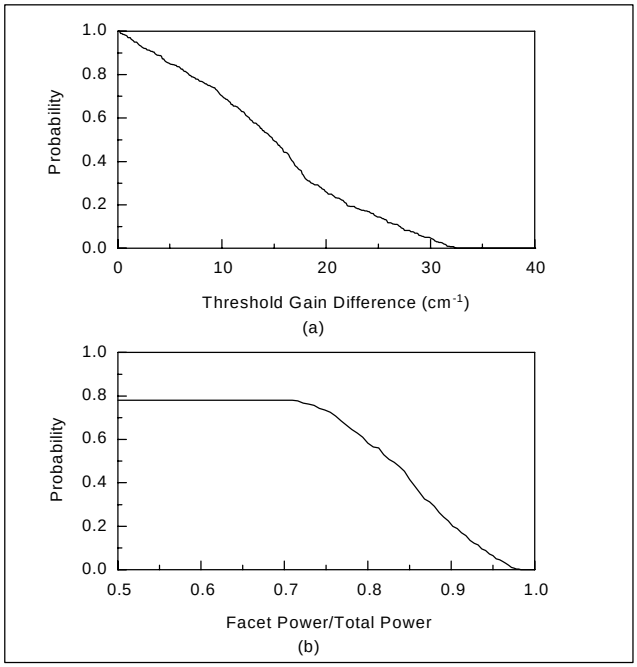

Fig. 7. Theoretical distributions of (a) threshold gain difference and (b) power extraction efficiency of the AR-HR coated ASG laser. The length of sections A and B are 100 μm and 300 μm, respectively.

gap mode could be used to obtain a high SMSR for the AR-HR coated ASG laser if the length of each section is well adjusted.

Figure 7 shows the threshold gain difference and the power extraction efficiency of the AR(1%)-HR(90%) coated ASG laser with section lengths of L_A=100 μm and L_B=300 μm. A single mode criterion was obtained at $\Delta g > 7.5$ cm^{-1} for the shortened cavity length. The single mode performance was obtained for 78% of the devices. In addition, more than 50% of the devices have a power extraction efficiency larger than 0.8, which means that the front facet power is 4 times larger than the rear facet power. Thus, we were able to obtain high power extraction efficiency from one of the facets without losing the single mode property.

IV. DESIGN OF A MULTI-WAVELENGTH ASG LASER ARRAY

The ASG laser described in the previous section can be used to easily fabricate an MLA by a means of the sampled grating because of its tunablility of the lasing wavelength. Figure 8 shows the schematic for an ASG laser array, where each laser has two sampled grating mirrors. The laser emits light at a wavelength where the two reflection spectra overlap, which is the –1st order reflection resulting from both the ASGs and the index shifter.

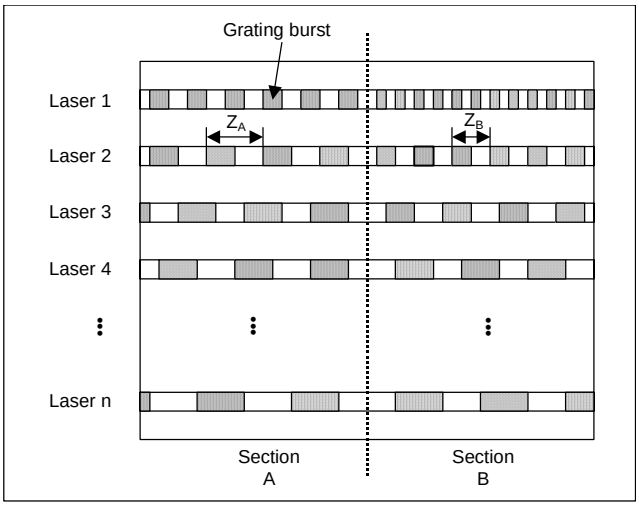

Fig. 8. Schematic of a multi-wavelength ASG laser array.

For the overlap of –1st order reflections, the sampling periods of the n-th laser should follow the relations of

$$Z_A^n = \frac{(\lambda_o^A)^2}{2n_{eff}(\lambda_o^A - \lambda_n)}, \qquad Z_B^n = \frac{(\lambda_o^B)^2}{2n_{eff}(\lambda_o^B - \lambda_n)} \qquad (6)$$

where λ_n is the emission wavelength of the n-th laser.

In our design, the total number of available wavelengths in the array depends on the range of the sampling period that is practical for the device fabrication and for obtaining acceptable device characteristics. The active medium has enough gain bandwidth that covers all –1st order reflection peaks. In Fig. 9, the sampling periods of sections A and B are plotted on the basis of (6). The channel spacing was 100 GHz (0.8 nm) and the center wavelength was 1550 nm. The maximum value of the sampling period is typically limited by the allowable length of the device, so we assumed it to be 50 μm. For reliable process control, the difference between Z_A and Z_B should not be too small. We assumed it to be 1.5 μm. Under the assumptions, 30 channels with 100 GHz spacing, which cover 24 nm, were realized by the ASG laser array. It should be stressed that a wide tuning range of 24 nm can be achieved without any adjustment to the material or the grating pitch.

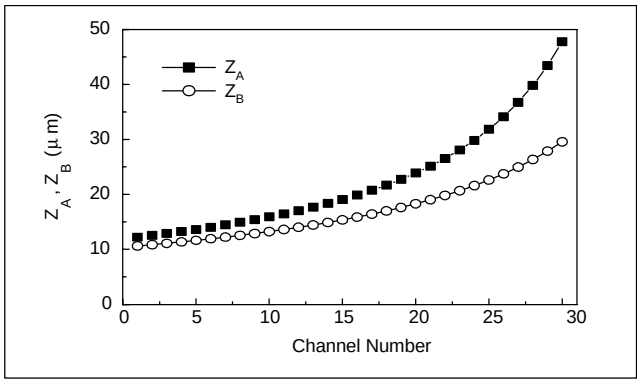

Fig. 9. Variation of sampling period vs. channel number for the MLA.

V. CONCLUSION

We proposed a novel design of an ASG laser along with a multi-wavelength laser array associated with it. With this design, one can fabricate an MLA with a single-period grating in a simple process with high yield. Theoretical simulation showed that the asymmetric sampled grating combined with the index shifter allowed the ASG laser to operate at the –1st order reflection. When HR-AR facet coatings were applied, the ASG laser produced high power extraction efficiency without losing its single mode property. For the MLA, the wavelength control was obtained by varying the sampling periods from laser to laser. With this design, we showed the feasibility of an array of up to 30 channels with a 100 GHz wavelength spacing.

REFERENCES

[1] K. Lee, K.C. Kong, T. Lee, and S. Park, "An Optimization Approach to Routing and Wavelength Assignment in WDM All-

Optical Mesh Networks without Wavelength Conversion," *ETRI J.*, vol. 24, no. 2, 2002, pp. 131-141.

[2] M. Yanagisawa, T. Hashimoto, F. Ebisawa, T. Kitagawa, H. Takahashi, A. Himeno, A. Sugita, Y. Yamada, and K. Okamoto, "A 2.5 Gb/s Hybrid Integrated Multiwavelength Light Source Composed of Eight DFB-LD's and an MMI Coupler on a Silica PLC platform," *24th European Conf. on Optical Communication 1998*, vol. 1, 1998, pp. 77-78.

[3] B. Pezeshki, A. Mathur, S. Zou, H.-S. Jeon, V. Agrawal, and R.L. Lang, "12 nm Tunable WDM Source Using an Integrated Laser Array," *Electron. Lett.*, vol. 36, no. 9, 2000, pp. 788-789.

[4] K. Kudo, T. Morimoto, K. Yashiki, T. Sasaki, Y. Yokoyama, K. Hamamoto, and M. Yamaguchi, "Wavelength-Selectable Microarray Light Sources of Multiple Ranges Simultaneously Fabricated on Single Wafer," *Electron. Lett.*, vol. 36, no. 8, 2000, pp. 745-747.

[5] Y. Katoh, T. Kunii, Y. Matsui, H. Wada, T. Kamijoh, and Y. Kawai, "DBR Laser Array for WDM System," *Electron. Lett.*, vol. 29, no. 25, 1993, pp. 2195-2197.

[6] S.-L. Lee, I.-F. Jang, C.-Y. Wang, C.-T. Pien, and T.-T. Shih, "Monolithically Integrated Multiwavelength Sampled Grating Lasers for Dense WDM Applications," *IEEE J. Selected Topics Quantum Electron.*, vol. 6, no. 1, 2000, pp. 197-206.

[7] B. Mason, G.A. Fish, S.P. DenBaars, and L.A. Coldren, "Widely Tunable Sampled Grating DBR Laser with Integrated Electroabsorption Modulator," *IEEE Photon. Technol. Lett.*, vol. 11, no. 6, 1999, pp. 638-640.

[8] Y. Tohmori, Y. Yoshikuni, H. Ishii, F. Kano, T. Tamamura, Y. Kondo, and M. Yamamoto, "Broad-Range wAvelength-Tunable Superstructure Grating (SSG) DBR Lasers," *IEEE J. Quantum Electron.*, vol. 29, no. 6, 1993, pp. 1817-1823.

[9] T. Fessant, "Influence of a Nonuniform Coupling Coefficient on the Static and Large Signal Dynamic Behavior of Bragg-Detuned DFB Lasers," *J. Lightwave Technol.*, vol. 16, no. 3, 1998, pp. 419-427.

[10] L.A. Coldren and S.W. Corzine, *Diode Lasers and Photonic Integrated Circuits*, John Wiley & Sons, Ch. 3, pp. 65-110.

[11] Y. Nakano, Y. Uchida, and K. Tada, "Highly Efficient Single Longitudinal-Mode Oscillation Capability of Gain-Coupled Distributed Feedback Semiconductor Lasers – Advantage of Asymmetric Facet Coating," *IEEE Photon. Technol. Lett.*, vol. 4, no. 4, 1992, pp. 308-310.

[12] P.P.G. Mols, P.I. Kuindersma, W.V. Es-Spiekman, and I.A.F. Baele, "Yield and Device Characteristics of DFB Lasers: Statistics and Novel Coating Design in Theory and Experiment," *IEEE J. Quantum Electron.*, vol. 25, no. 6, 1989, pp. 1303-1313.

[13] C.H. Henry, "Performance of Distributed Feedback Lasers Designed to Favor the Energy Gap Mode," *IEEE J. Quantum Electron.*, vol. QE-21, no. 12, 1985, pp. 1913-1918.

Sang-Wan Ryu was born in Korea on March 5, 1970. He received the BS, MS, and the PhD degrees in physics from Seoul National University, Seoul, Korea, in 1992, 1994, and 1998, respectively. After graduation, he joined the University of Southern California, Los Angeles, USA, as a post-Doc, where he worked on a long-wavelength VCSEL. He moved to the Electronics and Telecommunication Research Institute, Korea, in 2000, and has been continuing his research on an integrated WDM transmitter for metro and access networks.

Jeha Kim received the BS and MS degrees in physics from Sogang University, Seoul, South Korea in 1982 and 1985, respectively and the PhD degree in physics from University of Arizona, Tucson Arizona, USA in 1993. He joined Electronics and Telecommunications Research Institute, Daejeon, South Korea in 1993, where he worked at the Optoelectronics Section in the development of 10 Gbit/s Laser diode for optical communications. During 1995-1998, he worked on the high temperature superconducting (HTS) passive and active microwave devices for high sensitivity wireless communications. His current research interests are in the development of functional optoelectronic devices for WDM and OTDM fiber-optic communications and radio-on-fiber (ROF) link wireless system. He is now the Team Leader of the Integrated Optical Source Team and a Principal investigator in the projects of hybrid integrated wavelength selectable WDM optical source module and 60 GHz analog optical transceiver module for RF/optic conversion.